electrochem

MDPI

Article

Charge Transfer Rates Controlled by Frequency Dispersion of Double-Layer Capacitances

Koichi Jeremiah Aoki and Jingyuan Chen *

Electrochemistry Museum, Kofu 400-0015, Japan; d930099@yahoo.co.jp
* Correspondence: jingyuanchn46@yahoo.co.jp; Tel.: +81-9082625425

Abstract

Reported rate constants of charge transfer reactions (CTs) have ranged widely, depending on techniques and timescales. This fact can be attributed to the time-dependent double-layer capacitance (DLC), caused by solvent interactions such as hydrogen bonds. The time variation of the DLC necessarily affects the heterogeneous electrode kinetics. The delay by the solvation, being frequency dispersion, is incorporated into the CT kinetics in this report on the basis of the conventional reaction rate equations. It is different from the absolute rate theory. This report insists on a half value of the transfer coefficient owing to the segregation of the electrostatic energy from the chemical one. The rate equation here is akin to the Butler–Volmer one, except for the power law of the time caused by the delay of the DLC. The dipoles orient successively other dipoles in a group associated with the delay, which resembles that in the DLC. The delay suppresses the observed currents in the form of a negative capacitance. The above behavior was examined with a ferrocenyl derivative by ac impedance methods. The delay from diffusion control was attributed to the negative capacitance rather than the CT, even if the conventional DLC effect was corrected.

Keywords: charge transfer kinetics; double-layer capacitance; long-term interaction among solvents; ac impedance; negative capacitance

check for updates

Academic Editor: Masato Sone

Received: 25 July 2025
Revised: 16 August 2025
Accepted: 1 September 2025
Published: 5 September 2025

Citation: Aoki, K.J.; Chen, J. Charge Transfer Rates Controlled by Frequency Dispersion of Double-Layer Capacitances. *Electrochem* **2025**, *6*, 32. https://doi.org/10.3390/electrochem6030032

Copyright: © 2025 by the authors. Licensee MDPI, Basel, Switzerland. This article is an open access article distributed under the terms and conditions of the Creative Commons Attribution (CC BY) license (https://creativecommons.org/licenses/by/4.0/).

1. Introduction

Observed rates of a simple electrode reaction are composed of steps of (1) charge transfer, (2) mass transfer, and (3) solvation of the redox species, according to a conventional concept for charge transfer. They are accompanied by (4) charge–charge interactions as a latent step. Successively occurring steps could be partially distinguished so that the slowest step would be observed. However, actual steps are coupled. The frequent coupling is a combination of (1) and (2), which has been elucidated with the diffusion-corrected Butler–Volmer equation. Unfortunately, rates reported even for ferrocene have ranged from 0.02 to 220 cm s^{-1} [1], varying with techniques, conditions, and research groups. They may be complicated with rates of (3) and (4), which are relevant to a slow relaxation of double-layer capacitances.

Solvents in electrochemical processes have played a role in keeping high concentrations of redox species such as carbon powders [2,3], polymers [4–6], and battery materials [7–10]. The high solubility is attributed not only to simple physical properties of viscosity, dielectric constants, boiling and melting points, surface tensions, and solubility of ions but also complications by hydrogen bonding acidity, bipolarity, and a Hildebrand solubility parameter [11,12]. Static effects of solvents on redox reactions have

been revealed to standard potentials, exemplified with the potential dependence of ferrocenyl derivatives [13,14] and C_{60} [15–17]. In contrast, a large number of dynamical solvent effects have been reported in practical work on mixed solvents. However, their physicochemical reasons have not been discussed well. Even without redox species, the solvent effects have been exhibited in the double-layer capacitances (DLCs) through the wetting abilities of solvents [18], participation in field-oriented solvent dipoles [19], combinations of ionic liquids [20], and dependence on solvent conductivity and viscosity [21].

Electrode kinetics vary with the viscosity of solvents [22], their polarization [23,24], solvent-driven reorganization energy at the metal coordination [25,26], and diffusion coefficients through weak coordination [27,28]. A property common to these kinetic effects is a long period for the reorganization of solvent dipoles surrounding a redox molecule [23], as has been expressed in an easy-to-digest term, 'stickiness' [26]. The delay by solvent dipoles has also been found in the DLC as the power law of the frequency [29–31]. The delay has been explained with the constant phase elements [32–36], resistive capacitive contributions of field-driven ionic separation [36], and non-uniform current distribution by surface roughness [37]. Similar behavior has been reported in other fields as the comparison of diffusion distances [38] with the movable distance of a molecule and that of reaction rates [38] with the collision frequency of molecules.

A simple charge transfer (CT) of an electrode reaction normally undergoes the following four steps:

(a) Change in the charge of a redox molecule by a high electric field at the electrode–solution interface;
(b) Formation of a dipole by a counterion for charge neutralization;
(c) Rearrangement in terms of solvent dipoles for stabilization, like in the DLC;
(d) Current is produced by the flux of the redox concentration at the electrode.

Processes (a) and (b) are caused by the motion of one particle, whereas (c) and (d) are caused by mass behavior. Therefore, the observed rate is controlled with steps (c) and (d). The rearrangement (c) of the DLC is obeyed by the power law of the time, t^{λ}, for a positive value of λ close to zero [19,29–31]. An electrode potential can control the activity of the redox species through the Nernst equation, and then the activity is converted into concentrations [39] through (c) as a result of interaction among solvents.

The delay associated with the conversion of the activity to the concentration will be incorporated into the one-electron CT kinetics in this report in the context of solvent interaction. The kinetic equation will be derived in the form of the conventional chemical reaction rates rather than the absolute rate theory. It will be applied to the ac impedance technique to obtain a practical form useful for applications and will be verified experimentally by the use of a ferrocenyl derivative.

2. Theory

2.1. Kinetic Equation with Dipole Interaction

Our electrode reaction involves the one-electron transfer, R ↔ O + e, at an electrode without chemical complications. The 'e' is not a molecule because of the instability in solution. The expression 'O + e' represents the presence of O in the state of the field, causing a reduction rather than a molecular collision of O with the electron in solution. When we express a state of the hole as H and that of the electron as E, the reaction can be rewritten in the form of a bimolecular reaction as

$$\mathrm{R} + \mathrm{H} \rightarrow \mathrm{O}\ (k_{\mathrm{f}}) \text{ and } \mathrm{O} + \mathrm{E} \rightarrow \mathrm{R}\ (k_{\mathrm{b}}) \tag{1}$$

where k_f and k_b are the forward and backward rate constants, respectively. These states are controlled not only by electrode voltage but also by the environments of H and E, such as solvation and/or charge neutralization by salts. They are different from those in a vacuum, as can be imagined by the dependence of redox potentials on kinds of solvents and salts. The surface concentration of R, Γ_R, is generated from a supply of volume concentration of O, c_{Os}, multiplied by the intensity of the reductive state of H, and is consumed by the amount of that of R, c_{Rs}, multiplied by the intensity of the oxidative state of E, where the subscript 's' in c_s means the concentration at the electrode surface. Since the intensive quantities of H and E are equivalent to the number of the active reaction sites per area, they can be represented as surface concentrations, Γ_H, and Γ_E for H and E, respectively. Then, the rate equation becomes

$$d\Gamma_R/dt = k_b\, c_{Os}\, \Gamma_E - k_f\, c_{Rs}\, \Gamma_H \tag{2}$$

where a unit of k_k and k_b is, for example, $mol^{-1}\ m^3\ s^{-1}$.

When voltage V is applied to the electrode, a fraction of V, βV for $0 < \beta < 1$, contributes to the oxidation by the electrostatic energy $-\beta Ve$. In contrast, the remaining V, $(1-\beta)V$, is due to the reduction by $(1-\beta)Ve$. The densities of the reaction sites, H and E, seem to be proportional to their Boltzmann distributions in order to express the energy in terms of concentrations. The term consisting of the Boltzmann factor represents activity rather than the concentration, which includes interaction with solvents or salts for electric neutralization. Interaction of the redox charge with solvents, especially water, causes a macroscopic delay as long as 1 s, given by the power law of the time, $(t/t_0)^\lambda$ in the DLC [19,30,31], where t_0 is a standard time and λ is a constant close to zero. The time delay is required to convert the activity to the concentration [40]. Then, Γ_H and Γ_E can be reformed as

$$\Gamma_H = (t/t_0)^\lambda\, A_H \exp(\beta Ve/k_BT) \tag{3}$$

$$\Gamma_E = (t/t_0)^\lambda\, A_E \exp[-(1-\beta)Ve/k_BT] \tag{4}$$

where k_B is the Boltzmann constant and A_H and A_E are constants, including the chemical activation energy.

The logarithm of Equation (3) has the form of $\ln\Gamma_H(t/t_0)^{-\lambda} = \ln A_H + \beta Ve/k_BT$. The first term on the right-hand side represents the chemical activation energy, whereas the second one represents the electrostatic energy. The whole energy, $\ln\Gamma_H(t/t_0)^{-\lambda}$, is given by a simple sum of the two energies. The simple sum has been classically used for the definition of electrochemical potentials. Complete separation into the two energies implies that the electrostatic energy should provide either the oxidation state or the reduction one with equal probability without chemical properties. As a result, we have $\beta = 1-\beta$, or $\beta = 1/2$. Inserting Equations (3) and (4) into Equation (2) and using the current density, $j = -Fd\Gamma_R/dt$, we have

$$j/F = (t/t_0)^\lambda[k_f\, A_H\, c_{Rs}\, e^{VF/2RT} - k_b\, A_E\, c_{Os}\, e^{-VF/2RT}] \tag{5}$$

The rate has been assumed to be a first-order reaction with respect to the reactants, whereas the dipole interaction may occur with a high order of dipoles. The latter can be represented by $(t/t_0)^\lambda$. The equilibrium occurs for $V = V_e$, $c_{Rs} = c_R{}^*$ (the bulk concentration) and $c_{Os} = c_O{}^*$ at $j = 0$, satisfying

$$k_f\, A_H\, c_R{}^* \exp(V_eF/2RT) = k_b\, A_E\, c_O{}^* \exp(-V_eF/2RT) \tag{6}$$

We can rewrite Equation (5) as

$$j = (t/t_0)^{\lambda}\, F\Lambda(\mathrm{e}^{\eta/2}\, c_{\mathrm{Rs}}/c_{\mathrm{R}}{}^{*} - \mathrm{e}^{-\eta/2}\, c_{\mathrm{Os}}/c_{\mathrm{R}}{}^{*}) \tag{7}$$

where $\eta = F(V - V_{\mathrm{e}})/RT$ and

$$\Lambda = (k_{\mathrm{b}} k_{\mathrm{f}} A_{\mathrm{H}} A_{\mathrm{E}}\, c_{\mathrm{O}}{}^{*} c_{\mathrm{R}}{}^{*})^{1/2} \tag{8}$$

Here, a typical unit of Λ is mol m^{-2} s^{-1}. Equation (7) is a general CT kinetic equation independent of any electrochemical technique. Equation (7) has the same form as the Butler–Volmer (BV) equation if substitutions of $A_{\mathrm{H}}A_{\mathrm{E}} = 1$ and $F(k_{\mathrm{b}}k_{\mathrm{f}}c_{\mathrm{O}}{}^{*}c_{\mathrm{R}}{}^{*})^{1/2} = j_0$ (the exchange current density) are made for the transfer coefficient 0.5 and $\lambda = 0$.

The prediction of $\beta = 1/2$ infers an equal contribution of the electrostatic energy to both the oxidation and the reduction. In order to demonstrate this equality, we define the current densities of the oxidation and the reduction for a long time ($t \approx t_0$) in uniform concentrations as $j_{\mathrm{O}} = F\Lambda\, \mathrm{e}^{\beta\eta}$ and $j_{\mathrm{R}} = F\Lambda\, \mathrm{e}^{(1-\beta)\eta}$, respectively, in Equations (2) and (4). The derivatives with the potential, being admittance, become

$$\mathrm{d}j_{\mathrm{O}}/\mathrm{d}\eta = F\Lambda\beta\mathrm{e}^{\beta\eta} \tag{9}$$

$$\mathrm{d}j_{\mathrm{R}}/\mathrm{d}\eta = F\Lambda(1-\beta)\mathrm{e}^{(1-\beta)\eta} \tag{10}$$

The equality, $\mathrm{d}j_{\mathrm{O}}/\mathrm{d}\eta = \mathrm{d}j_{\mathrm{R}}/\mathrm{d}\eta$, only holds when $\beta = 1/2$.

Equation (7) is applied here to a voltage-controlled technique under the linear diffusion of O and R with a common value of the diffusion coefficient D. Inserting the relations of concentrations at the surface with the current density

$$c_{\mathrm{Os}} = c_{\mathrm{O}}{}^{*} + \{1/F(\pi D)^{1/2}\}\int_0{}^{t} j(t-u)u^{-1/2}\mathrm{d}u \tag{11}$$

$$c_{\mathrm{Rs}} = c_{\mathrm{R}}{}^{*} - \{1/F(\pi D)^{1/2}\}\int_0{}^{t} j(t-u)u^{-1/2}\mathrm{d}u \tag{12}$$

into Equation (6), we have

$$j(t/t_0)^{-\lambda}/F\Lambda = 2\sinh(\eta/2) - [\mathrm{e}^{\eta/2}/c_{\mathrm{R}}{}^{*} + \mathrm{e}^{-\eta/2}/c_{\mathrm{O}}{}^{*}]\int_0{}^{t} j(t-u)u^{-1/2}\mathrm{d}u/F(\pi D)^{1/2} \tag{13}$$

If $F\Lambda$ is regarded as the exchange current density at $\lambda = 0$, Equations (9) and (10) have the same form as the concentration-included BV for $\beta = 1/2$.

2.2. AC Impedance

We derive expressions for ac currents responding to the sinusoidal voltage with the overpotential $V - V_{\mathrm{e}}$ at the frequency f or the angular velocity $\omega = 2\pi f$. The integral in Equation (9) for the ac current density, $j = |j|\mathrm{e}^{i\omega t}$, becomes

$$\int_0{}^{t} j(u)(t-u)^{-1/2}\mathrm{d}u \approx |j|\mathrm{e}^{i\omega t}\int_0{}^{\infty}\mathrm{e}^{-i\omega u}u^{-1/2}\mathrm{d}u = |j|\mathrm{e}^{i\omega t}(\pi/2\omega)^{1/2}(1-i) \tag{14}$$

By use of approximations of $\sinh(\eta/2) \approx \eta/2$ and $\mathrm{e}^{\pm\eta/2} \approx 1$ for a small value of $\eta = F(V - V_{\mathrm{e}})/RT$ as well as the relation

$$1/c_{\mathrm{R}}{}^{*} + 1/c_{\mathrm{O}}{}^{*} = (4/c^{*})\cosh^{2}(\zeta_{\mathrm{dc}}/2) \tag{15}$$

Equation (13) is simplified to

$$\eta = j\{4(1 - i)\cosh^2(\zeta_{dc}/2)/c^*F(2D\omega)^{1/2} + (\omega/\omega_0)^{\lambda}/F\Lambda\} \quad (16)$$

where t and t_0 are replaced by $1/\omega$ and $1/\omega_0$, respectively, $\zeta_{dc} = F(E_{dc} - E^o)/RT\}$ for the dc voltage E_{dc}, and $c^* = c_O^* + c_R^*$. The kinetic real impedance Z_1 and the imaginary one Z_2, defined by $Z = Z_1 + iZ_2 = (RT/F)\eta/j$ are

$$Z_1 = (RT/F^2\Lambda)(\omega/\omega_0)^{\lambda} + 1/\sigma\omega^{1/2} \quad (17)$$

$$Z_2 = -1/\sigma\omega^{1/2} \quad (18)$$

where

$$\sigma = c^*F^2D^{1/2}\,\mathrm{sech}^2(\zeta_{dc}/2)/2^{3/2}RT \quad (19)$$

Z_2 expresses the impedance caused by diffusion. On the other hand, the CT term can be extracted from the following sum:

$$Z_1 + Z_2 = (f/f_0)^{\lambda}RT/F^2\Lambda \quad (20)$$

If plots of $\log(Z_1 + Z_2)$ against $\log f$ fall on a line, the slope provides λ. The intercept at $f = f_0$, for example, $f_0 = 1$ Hz, provides Λ through $\log(RT/F^2\Lambda)$. The specific case for $\lambda = 0$ expresses the conventional ac impedance analysis, as shown in Figure 1. The difference between (a) from the BV (c) in Figure 1 is remarkable in the high-frequency domain, where the kinetic effect is discerned from the diffusion behavior (b).

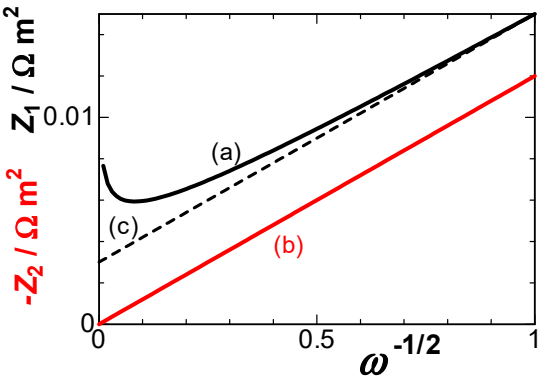


Figure 1. Variations of (a) Z_1 and (b) $-Z_2$ with $\omega^{-1/2}$, calculated from Equations (17) and (18), respectively, at $\lambda = 0.1$, $c_R^* = c_O^* = 1$ mM, $D = 10^{-5}$ cm^2 s^{-1}, and $RT/F^2\Lambda = 0.003\ \Omega$ m^2. (c) Represents Z_1 for the BV kinetics ($\lambda = 0$).

2.3. Contribution of Negative Capacitance

Electrode kinetics is necessarily disturbed by the current of the DLC because the capacitive current is largely involved in observed currents in such a high-frequency domain that the kinetics may be remarkable. This disturbance can be predicted from the conventional equivalent circuit in Figure 2, except for NC, where *W*b is the Warburg impedance and R_s is the solution resistance. The other obstacle to the kinetics is the negative capacitance [31] (NC), which is brought about with relaxation of the CT associated with rearrangements of solvent dipoles. The NC current flows in the direction opposite to the DLC current because of the inverse orientation of solvent dipoles. Since the NC has a form similar to the DLC, except for the sign, the admittance of the NC can be expressed as

$$Y_{NC} = (\lambda + I\,)\omega C_{NC} = (\lambda + i)C_{NC,1Hz}\,\omega^{1-\lambda}\omega_0{}^{\lambda} \quad (21)$$

where $C_{NC,1Hz}$ is a negative value of the NC at 1 Hz. The NC current is proportional to any faradaic current, including the diffusion-controlled currents, irrespective of the extent of kinetics. The observed current decreases by the amount of the NC current because it can be regarded as a parallel combination with the NC in the equivalent circuit, as shown in Figure 2. Then, the corrected admittance for the NC is $Y'' = Y' + Y_{NC}$, where Y' is the admittance corrected for the solution resistance and the DLC.

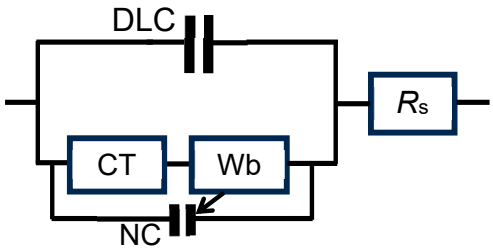


Figure 2. Equivalent circuit of the combination of impedance of the CT step, the diffusion (Wb), the DLC, the NC, and R_s.

3. Experimental Results and Discussion

The ac impedance was obtained with the application of ac voltage with a 10 mV amplitude and frequency ranging from 0.5 Hz to 5 kHz for the working electrode of a platinum wire 0.5 mm in diameter inserted into a test solution 5 mm long, as written previously [40]. The test solution was 1 mM (ferrocenylmethyl)trimethylammonium (FcTMA) + 0.5 M KCl to be deaerated before the electrochemical measurements. The reference electrode was Ag | AgCl in 0.5 M KCl.

3.1. Voltammetric Features

Nyquist plots at all the applied dc potentials took lines, as shown in the left inset of Figure 3, with (R_s, slope) = (12 Ω, 3.8) and (10 Ω, 0.97) as well as E_{dc} = 0.20 V and 0.36 V, respectively. Their slopes at E_{dc} near E^0 were united, whereas those at E_{dc} far from E^0 were more than 6. The former means the diffusion-controlled step [41], while the latter means the DLC control associated with the frequency dispersion [19,28,35]. No kinetic evidence, such as the appearance of a semicircle, was found at any dc potential. According to the BV equation combined with diffusion, Z_1 and $-Z_2$ should have a linear relationship with $f^{-1/2}$, as shown in Figure 3 (a) and (b), respectively. The intercept of the line in $-Z_2$ vs. $f^{-1/2}$ was zero, implying complete diffusion control. On the other hand, that for Z_1 vs. $f^{-1/2}$ was 4.2 Ω, which seems to represent the CT resistance, $R_{CT} = RT/F^2Ak^0c^*$ [41], where k^0 is the standard rate constant. The calculated value of k^0 would be 0.7 cm s^{-1}. Since the values of the impedance included the solution resistance 10.5 Ω from the Nyquist plot, the net R_{CT} must take a negative value [40]. A possible reason for the negative value is a contribution of the charging current, which is more remarkable at higher frequencies. Currents of the DLC have to be subtracted from the observed currents.

The observed impedance of the simplest redox reactions is controlled not only by the CT rates mixed with diffusion but also by (I) the ohmic drop mainly in the solution, by (II) the delay caused by the DLC, and by (III) the NC associated with the faradaic currents [31]. The above data were also obtained at gold and carbon electrodes but included less reproducibility than at the platinum wire.

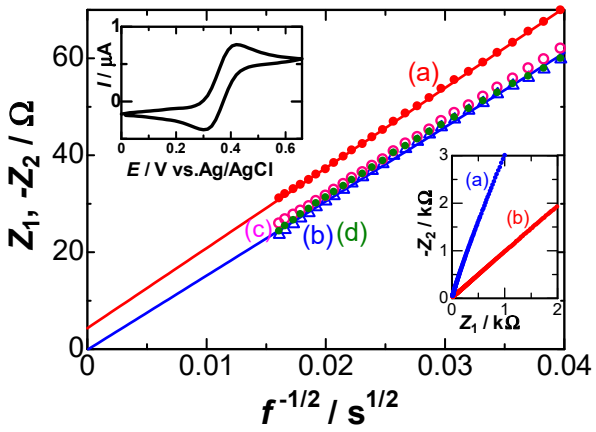


Figure 3. Randles plots of observed values of (a) Z_1 and (b) $-Z_2$ and corrected values of (c) Z_1' and (d) $-Z_2'$ at E_{dc} = 0.36 V vs. Ag | AgCl. The left inset is a voltammogram at a scan rate of 0.1 V s^{-1}. The right inset is Nyquist plots at E_{dc} = (a) 0.20 V and (b) 0.36 V.

3.2. Subtraction of the DLC

The ohmic resistance, R_s, was subtracted in the Nyquist plots from Z_1 by the use of the intercept on the Z_1-axis at extrapolated infinite frequency so that the corrected impedance was $Z_1 - R_s + iZ_2$. The observed DLC without FcTMA was almost independent of E_{dc}, Ref. [19] is opposed to the V-shape predicted by the Gouy–Chapman theory. This property allows us to apply the frequency-dependent DLC at the polarized potential to those at every depolarized potential. Since the DLC component is connected in parallel to the faradaic one at the equivalent circuit in Figure 2, admittance Y rather than impedance should be additive. $Z_1 - R_s + iZ_2$ was altered to Y (=$Y_1 + iY_2$), from which the two components of the DLC admittance, $Y_{1,DLC}$ and $Y_{2,DLC}$, were subtracted to yield Y'. Y' was transformed into the impedance $Z_1' + iZ_2'$. Variations of Z_1' and $-Z_2'$ with $f^{-1/2}$ are shown in Figure 3 (c), (d). The proportionality as well as the overlap of Z_1' and $-Z_2'$ implies the diffusion-controlled step without including any kinetics. Equations (17) and (18) indicate that $Z_1' + Z_2'$ should be logarithmically linear to the frequency. Figure 4 shows the plots at three values of E_{dc}, which deviated largely from a line predicted from Equations (17) and (18). Since the kinetic effect is exhibited more clearly at a higher frequency, we drew a line by force on the plots for log $f > 2$ in Figure 4 (b). The slope λ was less than 0.05, being as small as for an ideal capacitance ($\lambda = 0$). The intercepts varied largely with the applied potentials, inconsistent with Equations (17) adn (18). These unsatisfied results would be caused by the NC associated with faradaic reactions.

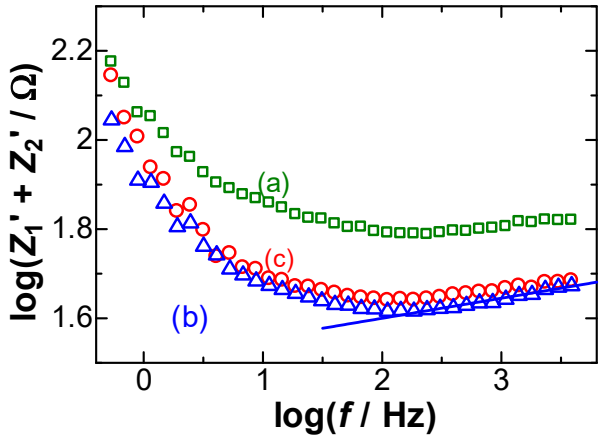


Figure 4. Logarithmic variations of the corrected values of $Z_1 + Z_2$ with f at E_{dc} = (a) 0.34, (b) 0.38, and (c) 0.40 V vs. Ag | AgCl.

3.3. Subtraction of Negative Capacitive Currents

If the ac current is controlled by diffusion, values of C_{NC} can be obtained through the logarithmic plots of $Y_1 - Y_2$ (=Y_{NC}) against f by the use of Equation (21). This analysis is based on the concept that the inequality, $Y_1 > Y_2$, is caused by the NC. Equation (21) can be rewritten as

$$(Y_1 - Y_2)_{NC} = -(1 - \lambda)C_{NC,1Hz}\ \omega^{1-\lambda}{\omega_0}^{\lambda} \tag{22}$$

where $C_{NC,1Hz}$ has a negative sign. On the other hand, the difference between Y_1 and Y_2 for the CT is given from Equation (21) by

$$(Y_1 - Y_2)_{CT} = \sigma\omega^{1/2}\chi/\{(1 + \chi)^2 + 1\} \tag{23}$$

where

$$\chi = \sigma\omega^{1/2}(\omega/\omega_0)^{\lambda}RT/F^2\Lambda \tag{24}$$

Since the value of χ for c^* = 1 mM, $D = 10^{-5}$ cm^2 s^{-1} and f = 1 kHz, a monomolecular layer adsorption for Λ (=10^{-9} mol cm^{-2} s^{-1}) is close to 100, and $Y_1 - Y_2$ is simplified to

$$(Y_1 - Y_2)_{CT} \approx \sigma\omega^{1/2}/\chi = (\omega/\omega_0)^{-\lambda}F^2\Lambda/RT \tag{25}$$

Subtracting Equations (22) and (23) from the R- and DLC-corrected admittance, Y', yields

$$Y_1'' - Y_2'' = (\lambda - 1)C_{NC,1Hz}\ \omega^{1-\lambda}{\omega_0}^{\lambda} + (\omega/\omega_0)^{-\lambda}F^2\Lambda/RT \tag{26}$$

Figure 5 shows logarithmic plots of the observed values of $Y_1'' - Y_2''$ against f for three values of E_{dc}. The linearity over the entire domain of log f indicates that either of the two terms on the right-hand side of Equation (26) should be valid. Positive values of the slopes (λ = 0.17) in Figure 5 suggest that $(Y_1 - Y_2)_{NC} >> (Y_1 - Y_{k2})_{CT}$. Therefore, the CT contribution for FcTMA is completely overtaken by the NC one. In other words, the plots in Figure 5 are represented as

$$\log(Y_1'' - Y_2'') = \log[(\lambda - 1)C_{NC,1Hz}] + (1 - \lambda)\log f \tag{27}$$

In order to confirm the significance of the NC term, we plotted the values of the intercept, $\log[(\lambda - 1)C_{NC,1Hz}]$, against E_{dc} in Figure 6. A bell shape was found, which was able to be approximated as $\log[\mathrm{sech}^2(\zeta_{dc}/2)]$. Since the potential dependence of $\mathrm{sech}^2(\zeta_{dc}/2)$ has been found in the diffusion-controlled ac currents [31], $C_{NC,1Hz}$ should be caused by the faradaic current of FcTMA. From the peak value of the curve at E_{dc} = 0.355 V vs. Ag | AgCl, we evaluated $C_{NC,1Hz} = -45$ μF cm^{-2}.

Of interest is a quantitative explanation of $(Y_1 - Y_2)_{NC} >> (Y_1 - Y_{k2})_{CT}$. Inserting Equations (22) and (23) into this inequality, we have

$$F\Lambda << (RT/F)\omega C_{NC,1Hz}\ (\lambda - 1)(\omega_0/\omega)^{2\lambda} \tag{28}$$

Equation (28) indicates that the CT rate becomes much smaller than the NC rate with the dependence of $\omega^{1-2\lambda}$ as the frequency is increased. Therefore, it is in vain to attempt to increase the frequency conventionally to determine high rates of the CT. Both Λ and $C_{NC,1Hz}$ are proportional to concentrations of the redox species [31]. As a result, it is difficult for us to distinguish the CT from the NC.

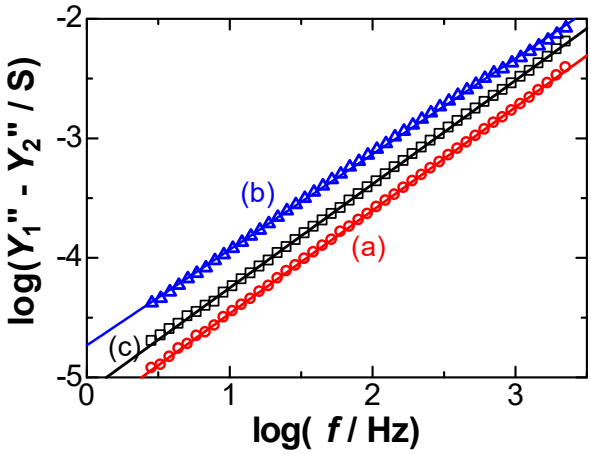


Figure 5. Logarithmic variations of corrected values of $Y_1'' - Y_2''$ with f at E_{dc} = (a) 0.30, (b) 0.36, and (c) 0.40 V vs. Ag | AgCl.

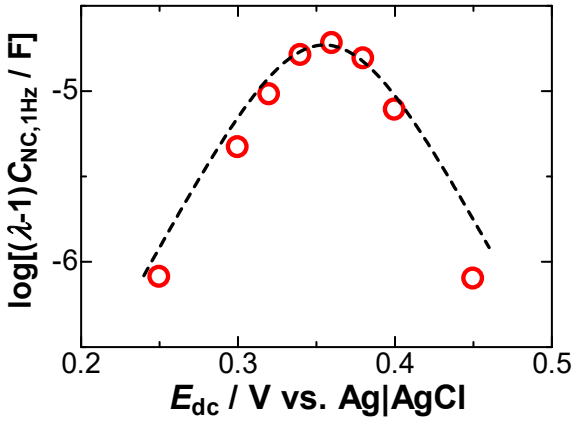


Figure 6. Variation of the intercept of lines in Figure 5 with E_{dc}. The dashed curve was calculated by curve fitting from $\log[\mathrm{sech}^2(\zeta_{dc}/2)]$.

4. Conclusions

The plots of Z_1 and Z_2 of raw impedance data against $f^{-1/2}$ lead to erroneous rate constants, although they have been conventionally used for evaluating rates. Even if impedance data are corrected for effects of solution resistance and the DLC, they show unpredicted frequency dependence of $f^{-\lambda}$ for the real impedance. The dependence arises from the delay in the conversion from the voltage-based activity to the concentration. Furthermore, the NC decreases the observed current. These two contributions should be considered for the CT kinetics.

The transfer coefficient in the BV is 1/2 if the electrostatic energy of the activation does not include any chemical properties. This conclusion is essential for the role of electrostatic energy, which should be segregated completely from chemical energy. Various values reported in Tafel slopes different from 0.5 suggest rate-determining steps irrelevant to the CT process.

Time-dependent measurements are necessarily complicated with capacitive currents because they include not only the DLC but also the NC. The current by the NC suppresses the observed diffusion current as if the kinetic current were to be included. It is difficult to distinguish the CT from the NC. Since the delay for FcTMA from diffusion control was attributed to the NC, no CT data could be obtained.

Author Contributions: Conceptualization, K.J.A.; methodology, J.C.; software, K.J.A.; validation, K.J.A. and J.C.; formal analysis, J.C.; investigation, K.J.A.; resources, K.J.A.; data curation, J.C.;

writing—original draft preparation, K.J.A.; writing—review and editing, K.J.A.; visualization, J.C.; supervision, J.C.; project administration, K.J.A.; funding acquisition, J.C. All authors have read and agreed to the published version of the manuscript.

Funding: This research received no external funding.

Institutional Review Board Statement: Not applicable.

Informed Consent Statement: Not applicable.

Data Availability Statement: Ask K.J.A. at d930099@yahoo.co.jp.

Conflicts of Interest: The authors declare no conflicts of interest.

References

1. Clegg, A.D.; Rees, N.V.; Klymenko, O.V.; Coles, B.A.; Compton, R.G. Marcus theory of outer-sphere heterogeneous electron transfer reactions: High precision steady-state measurements of the standard electrochemical rate constant for ferrocene derivatives in alkyl cyanide solvents. *J. Electroanal. Chem.* **2005**, *580*, 78–86. [CrossRef]
2. Rathinavel, S.; Priyadharshini, K.; Panda, D. A review on carbon nanotube: An overview of synthesis, properties, functionalization, characterization, and the application. *Mater. Sci. Eng. B* **2021**, *268*, 115095. [CrossRef]
3. Bergin, S.D.; Sun, Z.; Rickard, D.; Streich, P.V.; Hamilton, J.P.; Coleman, J.N. Multicomponent Solubility Parameters for Single-Walled Carbon Nanotube−Solvent Mixtures. *ACS Nano* **2009**, *3*, 2340–2350. [CrossRef]
4. Bone, J.M.; Jenkins, J.L. Understanding Polymer Electrodeposition and Conducting Polymer Modified Electrodes Using Electrochemistry, Spectroscopy, and Scanning Probe Microscopy. *J. Chem. Educ.* **2023**, *100*, 4062–4071. [CrossRef] [PubMed]
5. Gmucova, K. Fundamental aspects of organic conductive polymers as electrodes. *Cur. Opin. Electrochem.* **2022**, *36*, 101117. [CrossRef]
6. Vagin, M.; Che, C.; Gueskine, V.; Berggren, M.; Crispin, X. Ion-Selective Electrocatalysis on Conducting Polymer Electrodes: Improving the Performance of Redox Flow Batteries. *Adv. Funct Mater.* **2020**, *30*, 2007009. [CrossRef]
7. Romadina, E.I.; Stevenson, K.J. Small-Molecule Organics for Redox Flow Batteries—Creation of Highly-Soluble and Stable Compounds. *Electrochim. Acta* **2023**, *461*, 142670. [CrossRef]
8. Liao, H.; Zhong, W.; Li, T.; Han, J.; Sun, X.; Tong, X.; Zhang, Y. A review of self-healing electrolyte and their applications in flexible/stretchable energy storage devices. *Electrochim. Acta* **2022**, *404*, 139730. [CrossRef]
9. Belgibayeva, A.; Rakhmetova, A.; Rakhatkyzy, M.; Kairova, M.; Mukushev, I.; Issatayev, N.; Kalimuldina, G.; Nurpeissova, A.; Sun, Y.-K.; Bakenov, Z. Lithium-ion batteries for low-temperature applications: Limiting factors and solutions. *J. Power Sour.* **2023**, *557*, 232550. [CrossRef]
10. Pal, B.; Yang, S.; Ramesh, S.; Thangadurai, V.; Jose, R. Electrolyte selection for supercapacitive devices: A critical review. *Nanoscale Adv.* **2019**, *1*, 3807–3835. [CrossRef]
11. Lay, P.A. Specific hydrogen-bonding contributions to the thermodynamics and kinetics of electron transfer. Modifications to the classical and semiclassical theories of electron transfer. *J. Phys. Chem.* **1986**, *90*, 878–885. [CrossRef]
12. Barton, A.F.M. Solubility parameters. *Chem. Rev.* **1975**, *75*, 731–753. [CrossRef]
13. Noviandri, I.; Brown, K.N.; Fleming, D.S.; Gulyas, P.T.; Lay, P.A.; Masters, A.F.; Phillips, L. The Decamethylferrocenium/Decamethylferrocene Redox Couple: A Superior Redox Standard to the Ferrocenium/Ferrocene Redox Couple for Studying Solvent Effects on the Thermodynamics of Electron Transfer. *J. Phys. Chem. B* **1999**, *103*, 6713–6722. [CrossRef]
14. Hupp, J.T. The Ferrocene Assumption in Redox Thermodynamics: Implications from Optical Intervalence Studies of Ion Pairing to Ferrocenium. *Inorg. Chem.* **1990**, *29*, 5010–5012. [CrossRef]
15. Dubois, D.; Moninot, G.; Kutner, W.; Jones, M.T.; Kadish, K.M. Electroreduction of Buckminsterfullerene, C_{60}, in aprotic solvents. Solvent, supporting electrolyte, and temperature effects. *J. Phys. Chem.* **1992**, *96*, 7137–7145. [CrossRef]
16. Soucaze-Guillous, B.; Kutner, W.; Jones, M.T.; Kadish, K.M. Electroreduction of C_{60} in Aprotic Solvents: III. Voltammetric Study, at Microelectrode, of (n = 0 to 4) Solvation in the Absence of Supporting Electrolyte. *J. Electrochem. Soc.* **1996**, *143*, 550–556. [CrossRef]
17. Noviandri, I.; Bolskar, R.D.; Lay, P.A.; Reed, C.A. Solvent Effects on the Electrochemistry of C_{60}. Thermodynamics of Solvation of C_{60} and Fullerides. *J. Phys. Chem. B* **1997**, *101*, 6350–6358. [CrossRef]
18. Korchagin, O.V.; Bogdanovskaya, V.A.; Tripachev, O.V. Changes in double layer capacitance of the positive electrode in Li-O_2 battery during discharge: Effect of active material and aprotic electrolyte solvent. *J. Electroanal. Chem.* **2023**, *948*, 117815. [CrossRef]
19. Hou, Y.; Aoki, K.; Chen, J.; Nishiumi, T. Solvent Variables Controlling Electric Double Layer Capacitance at the Metal–Solution Interface. *J. Phys. Chem. C* **2014**, *118*, 10153–10158. [CrossRef]

20. Silvester, D.S.; Jamil, R.; Doblinger, S.; Zhang, Y.; Atkin, R.; Li, H. Electrical Double Layer Structure in Ionic Liquids and Its Importance for Supercapacitor, Battery, Sensing, and Lubrication Applications. *J. Phys. Chem. C* **2021**, *125*, 13707–13720. [CrossRef]
21. Arulepp, M.; Permann, L.; Leis, J.; Perkson, A.; Rumma, K.; Janes, A.; Lust, E. Influence of the solvent properties on the characteristics of a double layer capacitor. *J. Power Sour.* **2004**, *133*, 320–328. [CrossRef]
22. Zagrebin, P.A.; Buchner, R.; Nazmutdinov, R.R.; Tsirlina, G.A. Dynamic solvent effects in electrochemical kinetics: Indications for a switch of the relevant solvent mode. *J. Phys. Chem. B* **2010**, *114*, 311–320. [CrossRef]
23. Weaver, M.J. Dynamical Solvent Effects on Activated Electron-Transfer Reactions: Principles, Pitfalls, and Progresst. *Chemical Reviews* **1992**, *92*, 463–480. [CrossRef]
24. Weaver, M.J.; McManis III, G.E. Dynamical solvent effects on electron-transfer processes: Recent progress and perspectives. *Acc. Chem. Res.* **1990**, *23*, 294–300. [CrossRef]
25. Nazmutdinov, R.R.; Dudkina, Y.B.; Zinkicheva, T.T.; Budnikova, Y.H.; Probst, M. Ligand and solvent effects on the kinetics of the electrochemical reduction of Ni(II) complexes: Experiment and quantum chemical modeling. *Electrochim. Acta* **2021**, *395*, 139138. [CrossRef]
26. Fawcett, W.R.; Opallo, M. Possible experimental evidence for molecular solvation effects in simple heterogeneous electron-transfer reactions. *J. Phys. Chem.* **1992**, *96*, 2920–2924. [CrossRef]
27. Black, A.W.; Bartlett, P.N. Selection and characterisation of weakly coordinating solvents for semiconductor electrodeposition. *Phys. Chem. Chem. Phys.* **2022**, *24*, 8093–8103. [CrossRef]
28. Black, A.W.; Zhang, W.; Reid, G.; Bartlett, P.N. Diffusion in weakly coordinating solvents. *Electrochim. Acta* **2022**, *425*, 140720. [CrossRef]
29. Lasia, A. The Origin of the Constant Phase Element. *J. Phys. Chem. Lett.* **2022**, *13*, 580–589. [CrossRef]
30. Aoki, K.J. Molecular interaction model for frequency-dependence of double layer capacitors. *Electrochim. Acta* **2016**, *188*, 545–550. [CrossRef]
31. Aoki, K.J. Frequency-dependence of electric double layer capacitance without Faradaic reactions. *J. Electroanal. Chem.* **2016**, *779*, 117–125. [CrossRef]
32. Lasia, A. *Modern Aspects of Electrochemistry, 32*; Kluwer Academic/Plenum Publishers: New York, NY, USA, 1999; p. 143.
33. Brug, G.J.; Van den Eeden, A.L.G.; Sluyters-Rehbach, M.; Sluyters, J.H. The analysis of electrode impedances complicated by the presence of a constant phase element. *J. Electroanal. Chem.* **1984**, *176*, 275–295. [CrossRef]
34. Nyikos, L.; Pajkossy, T. Fractal dimension and fractional power frequency-dependent impedance of blocking electrodes. *Electrochim. Acta* **1985**, *30*, 1533–1540. [CrossRef]
35. Zoltowski, P. On the electrical capacitance of interfaces exhibiting constant phase element behavior. *J. Electroanal. Chem.* **1998**, *443*, 149–154. [CrossRef]
36. Schalenbach, M.; Durmus, Y.E.; Robinson, S.A.; Tempel, H.; Kungl, H.; Eichel, R.-A. Physicochemical Mechanisms of the Double-Layer Capacitance Dispersion and Dynamics: An Impedance Analysis. *J. Phys. Chem. C* **2021**, *125*, 5870–5879. [CrossRef]
37. Pajkossy, T.; Jurczakowski, R. Electrochemical impedance spectroscopy in interfacial studies. *Curr. Opin. Electrochem.* **2017**, *1*, 53–58. [CrossRef]
38. Atkins, P.; Paula, J.D. *Atkin's Physical Chemistry*, 10th ed.; Oxford University Press: Oxford, UK, 2023; pp. 811, 896–899, 915.
39. Liu, Y.; Aoki, K.J.; Chen, J. Similarity of Heterogeneous Kinetics to Delay of Double-Layer Capacitance Using Chronoamperometry. *Electrochem* **2023**, *4*, 301–312. [CrossRef]
40. Aoki, K.J.; Liu, Y.; Chen, J. Delay of reaching the Nernst equilibrium by ac-impedance. *J. Solid State Electrochem.* **2024**, *28*, 4503–4510. [CrossRef]
41. Bard, A.J.; Faulkner, L.R. *Electrochemical Methods*, 2nd ed.; Kohn Wiley & Sons: New York, NY, USA, 2001; pp. 381, 384–385.

Disclaimer/Publisher's Note: The statements, opinions and data contained in all publications are solely those of the individual author(s) and contributor(s) and not of MDPI and/or the editor(s). MDPI and/or the editor(s) disclaim responsibility for any injury to people or property resulting from any ideas, methods, instructions or products referred to in the content.